

# A particle-hole model approach for hypernuclei

M. Martini<sup>a,b</sup>, V. De Donno<sup>a</sup>, C. Maieron<sup>a</sup>, G. Co' <sup>a</sup>

<sup>a</sup> Dipartimento di Fisica, Università del Salento,  
and Istituto Nazionale di Fisica Nucleare sez. di Lecce,  
I-73100 Lecce, Italy

<sup>b</sup> Université de Lyon, F-69622, Lyon, France; Université Lyon 1, Villeurbanne;  
CNRS/IN2P3, UMR5822, Institut de Physique Nucléaire de Lyon

## Abstract

A particle-hole model is developed to describe the excitation spectrum of single  $\Lambda$  hypernuclei and the possible presence of collective effects is explored by making a comparison with the mean-field calculations. Results for the spectra of  ${}_{\Lambda}^{12}\text{C}$ ,  ${}_{\Lambda}^{16}\text{O}$ ,  ${}_{\Lambda}^{40}\text{Ca}$ ,  ${}_{\Lambda}^{90}\text{Zr}$  and  ${}_{\Lambda}^{208}\text{Pb}$  hypernuclei are shown. The comparison with the available experimental data is satisfactory. We find that collective phenomena are much less important in hypernuclei than in ordinary nuclei.

PACS: 21.80.+a

## 1 Introduction

The properties of hypernuclei have been widely studied in several experiments and today they are the object of a rich experimental program. The first experiments were aimed at identifying the hypernuclei and at determining the energy of the hyperon embedded in the nucleus. Presently, the improvement of the experimental techniques allows the measurement of high-quality excitation spectra, which have been studied in  $(\pi^+, K^+)$  [1, 2, 3, 4],  $(K^-, \pi^-)$  [5, 6, 7] or  $(e, e'K^+)$  [8, 9, 10] reactions. In the future, further advance in these studies will be gained by means of  $\gamma$ -ray spectroscopy, which will become a standard investigation tool [11, 12].

From the theoretical point of view, single- $\Lambda$  hypernuclei have been studied within the mean-field (MF) approximation: the hypernucleus is seen as a many-body system containing an impurity, and its properties are solely determined by those of the hyperon moving in an average potential generated by the interaction with the nucleons. When applied to various medium heavy nuclei, the MF model is quite successful in reproducing the single hyperon energies, which are single particle properties of the system. On the other hand, the excitation spectra of hypernuclei are, in general, related to the system as a whole.

In purely nucleonic nuclei there are large differences between the experimental excitation spectrum and that predicted by the MF model, where the excitation energies are simply given by the differences between the energies of the particle and hole states. This indicates that the many body-terms of the hamiltonian neglected in the MF approximation play a relevant role. It is therefore interesting to study also the excitation spectra of hypernuclei by using models beyond the simple MF approach.

In the past this kind of studies have been done within the Tamm Dancoff Approximation (TDA) [13, 14], which describes the many-body excited state as a linear combination of particle-hole excitations of a MF ground state. The theoretical inconsistencies of the TDA theory are overcome by the Random Phase Approximation (RPA) theory which considers some ground state correlations [15].

We have developed an RPA-like model which describes the spectra of single  $\Lambda$  hypernuclei. In our model, the hypernucleus is formed when a nucleon, from its state below the Fermi surface, a hole state, is transformed into a  $\Lambda$  which lies in one specific particle state. The excited state of the hypernucleus is a combination of various particle-hole excitations. This combination is ruled by the residual  $\Lambda$ -nucleon interaction. The relevance of the residual interaction, and therefore the possible presence of collective phenomena, is investigated by comparing MF results with those obtained by our model.

In the next section we present the details of the model. In Sect. 3 we describe how we have chosen the input of our calculations, namely the set of single particle wave functions and energies, and the effective  $\Lambda$ -nucleon interactions. A selected set of results concerning hypernuclei obtained from doubly-closed shell nuclei is discussed in Sect. 4. Finally, in Sect. 5 we summarize the basic findings of our study and draw our conclusions.

## 2 The formalism

The starting point of our model is the MF description of the many-body system. Each baryon is described by its single particle wave function  $\phi_\alpha$  and energy  $\epsilon_\alpha$ , where  $\alpha$  indicates the set of quantum numbers which identify the single particle level.

The definition of the single particle basis allows us to write the many-body hamiltonian as [15]

$$H = \sum_{\alpha} \epsilon_{\alpha} a_{\alpha}^{\dagger} a_{\alpha} - \frac{1}{2} \sum_{hh'} \bar{V}_{hh'hh'} + \frac{1}{4} \sum_{\alpha\alpha'\beta\beta'} \bar{V}_{\alpha\alpha'\beta\beta'} N \left[ a_{\alpha}^{\dagger} a_{\alpha'}^{\dagger} a_{\beta'} a_{\beta} \right] , \quad (1)$$

where we have indicated with  $a^{\dagger}$  and  $a$  the creation and annihilation operators, and with  $N$  the normal ordered product operator [16]. In the above equation, the bar over the interaction  $V$  indicates that both direct and exchange terms are considered, the  $h$  label identifies a state below the Fermi surface, while the Greek subindexes refer to states above or below the Fermi surface.

We describe the formation of the hypernucleus as a time dependent fluctuation of the MF ground state. We solve the time dependent Schrödinger equation by using the variational principle

$$\delta \left\{ \langle \Psi(t) | \left[ H - i\hbar \frac{\partial}{\partial t} \right] | \Psi(t) \rangle \right\} = 0 . \quad (2)$$

We search for the minimum of the above energy functional within the Hilbert subspace spanned by trial wave functions of the form

$$|\Psi(t)\rangle \rightarrow |\Phi(t)\rangle = e^{-iE_0 t/\hbar} \exp \left[ \sum_{\Lambda h} C_{\Lambda h}(t) a_{\Lambda}^{\dagger} a_h \right] |\Phi_0\rangle , \quad (3)$$

where  $|\Phi_0\rangle$  indicates the MF ground state of the system, formed by nucleons only. In equation (3) we have indicated with  $a_{\Lambda}^{\dagger}$  the operator which creates a  $\Lambda$ , and with  $a_h$  the operator annihilating a nucleon. The coefficients  $C_{\Lambda h}(t)$  are complex numbers.

By using the ansatz (3) in Eq. (2) we express the variational equation as

$$\frac{\partial}{\partial C_{\Lambda h}^*(t)} \langle \Phi(t) | \left[ H - i\hbar \frac{\partial}{\partial t} \right] | \Phi(t) \rangle = 0 . \quad (4)$$

By making a power expansion of the exponential of Eq. (3), and retaining only the terms up to the second order in  $C(t)$ , we obtain the expression [15]

$$\begin{aligned} C_{\Lambda h}(t)(\epsilon_{\Lambda} - \epsilon_h) &+ \sum_{\Lambda' h'} C_{\Lambda' h'}^*(t) \bar{V}_{\Lambda \Lambda' h h'} + \sum_{\Lambda' h'} C_{\Lambda' h'}(t) \bar{V}_{\Lambda h' h \Lambda'} \\ &= i\hbar \frac{d}{dt} C_{\Lambda h}(t) . \end{aligned} \quad (5)$$

Since we are looking for oscillating solutions, we write the coefficients as

$$C_{\Lambda h}(t) = W_{\Lambda h}e^{-i\nu t} + Z_{\Lambda h}^*e^{i\nu t} , \quad (6)$$

and by equating positive and negative frequencies components we obtain the equations

$$W_{\Lambda h}(\epsilon_{\Lambda} - \epsilon_h) + \sum_{\Lambda'h'} \bar{V}_{\Lambda h'h\Lambda'} W_{\Lambda'h'} + \sum_{\Lambda'h'} \bar{V}_{\Lambda\Lambda'hh'} Z_{\Lambda'h'} = \hbar\nu W_{\Lambda'h'} \quad (7)$$

$$Z_{\Lambda h}^*(\epsilon_{\Lambda} - \epsilon_h) + \sum_{\Lambda'h'} \bar{V}_{\Lambda h'h\Lambda'} Z_{\Lambda'h'}^* + \sum_{\Lambda'h'} \bar{V}_{\Lambda\Lambda'hh'} W_{\Lambda'h'}^* = -\hbar\nu Z_{\Lambda'h'}^* . \quad (8)$$

Introducing the matrix elements

$$H_{\Lambda h\Lambda'h'} = (\epsilon_{\Lambda} - \epsilon_h)\delta_{\Lambda\Lambda'}\delta_{hh'} + \bar{V}_{\Lambda h'h\Lambda'} \quad (9)$$

$$I_{\Lambda h\Lambda'h'} = \bar{V}_{\Lambda\Lambda'hh'} , \quad (10)$$

equations (7) and (8) can be expressed in the following matrix form

$$\begin{pmatrix} H & I \\ -I^* & -H^* \end{pmatrix} \begin{pmatrix} W \\ Z \end{pmatrix} = \omega \begin{pmatrix} W \\ Z \end{pmatrix} , \quad (11)$$

where we have defined  $\omega = \hbar\nu$ . We have rewritten the secular equations in a matrix form to show their similarity with the traditional RPA secular equations [17]. Our derivation of the secular equations shows that the  $W$  and  $Z$  amplitudes are introduced on equal footing, and that the choice of neglecting one of the two terms of Eq. (6) is a further approximation of the theory. On the other hand, the derivation of the secular equations done with the equation of motion method [15, 17] indicates that the  $Z$  amplitudes are related to ground state correlations. Neglecting the  $Z$  amplitudes produces TDA secular equations which have been used in the past [13, 14] to describe hypernuclei. A discussion on the relevance of the ground state correlations introduced by the  $Z$  amplitudes will be done at the beginning of section 4. However, we would like to point out here that the ground state correlations we include are only those described by  $\Lambda$ -nucleon excitations, and not by nucleon-nucleon excitations. For this reason our model does not include nucleonic correlations as it is done in the traditional RPA theory.

In our calculations the ground state of the nucleus and the final state of the hypernucleus have definite angular momentum values. For this reason we rewrite the above equations in angular momentum coupling scheme. The angular momentum coupled amplitudes are defined in terms of the uncoupled ones as

$$W_{\Lambda h}^J = \sum_{m_{\Lambda}m_h} \langle j_{\Lambda}m_{\Lambda}j_h m_h | JM \rangle W_{\Lambda h} \quad (12)$$

$$Z_{\Lambda h}^J = \sum_{m_{\Lambda}m_h} \langle j_{\Lambda}m_{\Lambda}j_h m_h | J - M \rangle (-1)^{J-M} Z_{\Lambda h} , \quad (13)$$

where the  $j$ 's indicate the total angular momentum characterizing the single particle wave functions and the  $m$ 's their z-axis components.

We express the terms (9 - 10) of the secular matrix (11) as

$$H_{\Lambda h\Lambda'h'}^J = (\epsilon_{\Lambda} - \epsilon_h)\delta_{\Lambda\Lambda'}\delta_{hh'} + v_{\Lambda h\Lambda'h'}^J \quad (14)$$

$$I_{\Lambda h\Lambda'h'}^J = u_{\Lambda h\Lambda'h'}^J , \quad (15)$$

where we have defined

$$\begin{aligned} v_{\Lambda h\Lambda'h'}^J &= v_{\Lambda h\Lambda'h'}^{Jdir} - v_{\Lambda h\Lambda'h'}^{Jexch} \\ &= \sum_K (-1)^{j_h+j_{\Lambda'}+K} \hat{K} \begin{Bmatrix} j_{\Lambda} & j_h & J \\ j_{\Lambda'} & j_{h'} & K \end{Bmatrix} \\ & \left[ \langle j_{\Lambda}j_h'K || V || j_hj_{\Lambda'}K \rangle - (-1)^{j_h+j_{\Lambda'}-K} \langle j_{\Lambda}j_h'K || V || j_{\Lambda'}j_hK \rangle \right] , \end{aligned} \quad (16)$$

and

$$u_{\Lambda h \Lambda' h'}^J = u_{\Lambda h \Lambda' h'}^{Jdir} - u_{\Lambda h \Lambda' h'}^{Jexch} = (-1)^{j_{h'} - j_{\Lambda'} - J} v_{\Lambda h h' \Lambda'}^J . \quad (17)$$

Here we use the notation

$$\hat{J} = \sqrt{2J+1} , \quad (18)$$

and the term in curly brackets is the Wigner  $6j$  coefficient. The double bar in the matrix elements in Eq. (16) indicates that in the calculation of the angular part we consider the reduced matrix element as defined by the Wigner-Eckart theorem [18].

In calculating the interaction matrix elements we use the Fourier transform of the interaction expressed in momentum space

$$v(|\mathbf{r}_1 - \mathbf{r}_2|) = \frac{1}{(2\pi)^3} \int d\mathbf{q} e^{i\mathbf{q} \cdot |\mathbf{r}_1 - \mathbf{r}_2|} [F_\Lambda(q) + G_\Lambda(q) \boldsymbol{\sigma}(1) \cdot \boldsymbol{\sigma}(2) + H_\Lambda(q) S_{12}(\mathbf{q})] , \quad (19)$$

where we have used  $q \equiv |\mathbf{q}|$  and we have indicated with  $\boldsymbol{\sigma}$  the Pauli spin matrices and with  $S_{12}$  the usual tensor operator [18]. The above expression allows us to separate the terms dependent on  $\mathbf{r}_1$  from those dependent on  $\mathbf{r}_2$ . The explicit expressions of the matrix elements for the various terms of the interaction are given in the Appendix. The solution of Eq. (11) provides the excitation energies  $\omega$  and also the wave function of the excited state.

We then consider the transition from the nucleus ground state to an excited state of the hypernucleus induced by a generic one-body operator  $T_J$ . The transition matrix element is given by

$$\begin{aligned} \langle J|T_J|0 \rangle = \sum_{\Lambda h} & \left[ W_{\Lambda h}^J \langle j_\Lambda || T_J || j_h \rangle \right. \\ & \left. + (-1)^{J+j_\Lambda-j_h} Z_{\Lambda h}^J \langle j_h || T_J || j_\Lambda \rangle \right] . \end{aligned} \quad (20)$$

For the natural parity states we use the operator

$$T_J = j_J(qr) Y_{JM}(\Omega) , \quad (21)$$

where  $j_J(qr)$  are the spherical Bessel function, and  $Y_{JM}$  the spherical harmonics. The matrix elements to be inserted in Eq. (20) are

$$\langle j_a || T_J || j_b \rangle = \int dr r^2 R_a^*(r) R_b(r) j_J(qr) \langle j_a || Y_J || j_b \rangle , \quad (22)$$

where  $R(r)$  is the radial part of the single particle wave function and

$$\begin{aligned} \langle j_a || Y_J || j_b \rangle & \equiv \langle l_a \frac{1}{2} j_a || Y_J || l_b \frac{1}{2} j_b \rangle \\ & = (-1)^{j_a + \frac{1}{2}} \frac{\hat{j}_a \hat{j}_b \hat{J}}{\sqrt{4\pi}} \begin{pmatrix} j_a & J & j_b \\ \frac{1}{2} & 0 & -\frac{1}{2} \end{pmatrix} \xi(l_a + l_b + J) . \end{aligned} \quad (23)$$

In the above equation we have used the Wigner 3-j symbol [18], and  $\xi(l) = 1$  if  $l$  is even, and 0 otherwise.

For the unnatural parity states we use the operators

$$T_{L=J\pm 1} = j_L(qr) [Y_L(\Omega) \otimes \boldsymbol{\sigma}(1)]_M^J , \quad (24)$$

therefore the matrix elements to be inserted in Eq. (20) are

$$\begin{aligned} \langle j_a || T_L || j_b \rangle = & \\ \int dr r^2 R_a^*(r) R_b(r) j_L(qr) & \langle j_a || [Y_L(\Omega) \otimes \boldsymbol{\sigma}(1)]^J || j_b \rangle , \end{aligned} \quad (25)$$

with

$$\begin{aligned} \langle j_a || [Y_{J+s} \otimes \sigma]^J || j_b \rangle &= (-1)^{l_a+l_b+j_b+\frac{1}{2}} \frac{\hat{j}_a \hat{j}_b}{\sqrt{4\pi}} \frac{\chi_a + \chi_b + sJ + \delta_{s,1}}{\sqrt{J + \delta_{s,1}}} \\ &\quad \begin{pmatrix} j_a & j_b & J \\ \frac{1}{2} & -\frac{1}{2} & 0 \end{pmatrix} \xi(l_a + l_b + J + 1) , \end{aligned} \quad (26)$$

where we have defined

$$\chi = (-1)^{l+j+\frac{1}{2}} \left( j + \frac{1}{2} \right) ,$$

and  $s = \pm 1$ .

We also consider the transition between two excited states of the hypernucleus induced by a generic one-body operator ( $EM$ ). By using standard techniques [17, 19] we obtain for the transition matrix elements

$$\begin{aligned} &\langle \Phi_\nu | (EM) | \Phi'_\nu \rangle \\ &= \sum_{\Lambda h} \sum_{\Lambda' h'} \delta_{hh'} \left[ W_{\Lambda h}^\nu W_{\Lambda' h'}^{\nu'} \langle \Lambda | (EM) | \Lambda' \rangle - Z_{\Lambda h}^\nu Z_{\Lambda' h'}^{\nu'} \langle \Lambda' | (EM) | \Lambda \rangle \right] \\ &- \sum_{\Lambda h} \sum_{\Lambda' h'} \delta_{\Lambda \Lambda'} \left[ W_{\Lambda h}^\nu W_{\Lambda' h'}^{\nu'} \langle h' | (EM) | h \rangle - Z_{\Lambda h}^\nu Z_{\Lambda' h'}^{\nu'} \langle h | (EM) | h' \rangle \right] . \end{aligned} \quad (27)$$

We calculate the electromagnetic transition probabilities between two states of the hypernucleus by using the expression [20]

$$\mathcal{T}_{if}^L = \frac{4k}{\hbar c^2 (2J_i + 1)(2L + 1)} |\langle J_f || (EM)_L || J_i \rangle|^2 \quad (28)$$

where the indexes  $i$  and  $f$  indicate, respectively, the initial and final state of the transition,  $k$  is the modulus of the emitted photon momentum, and  $(EM)_L$  is the electromagnetic operator, of multipolarity  $L$ . In the above equation, as before, the double bar indicates that we have to evaluate the reduced matrix element of the angular dependent part.

We find that, in the angular momentum coupling scheme, the reduced transition matrix element between the two excited states *i.e.* Eq. (27), can be written as

$$\begin{aligned} \langle J || (EM)_L || J' \rangle &= \hat{J} \hat{J}' \sum_{\Lambda h} \sum_{\Lambda' h'} \left\{ \delta_{hh'} \begin{Bmatrix} J' & L & J \\ j_\Lambda & j_h & j_{\Lambda'} \end{Bmatrix} \right. \\ &\quad \left[ (-1)^{j_\Lambda + j_h + J' + L} W_{\Lambda h}^J W_{\Lambda' h'}^{J'} \langle j_\Lambda || (EM)_L || j_{\Lambda'} \rangle \right. \\ &\quad \left. - (-1)^{j_{\Lambda'} + j_{h'} + J'} Z_{\Lambda h}^J Z_{\Lambda' h'}^{J'} \langle j_{\Lambda'} || (EM)_L || j_\Lambda \rangle \right] \\ &\quad - \delta_{\Lambda \Lambda'} \begin{Bmatrix} L & J' & J \\ j_\Lambda & j_h & j_{h'} \end{Bmatrix} \\ &\quad \left[ (-1)^{j_{\Lambda'} + j_h + J} W_{\Lambda h}^J W_{\Lambda' h'}^{J'} \langle j_{h'} || (EM)_L || j_h \rangle \right. \\ &\quad \left. \left. - (-1)^{j_\Lambda + j_{h'} + J' + L} Z_{\Lambda h}^J Z_{\Lambda' h'}^{J'} \langle j_h || (EM)_L || j_{h'} \rangle \right] \right\} . \end{aligned} \quad (29)$$

The expressions of the single particle matrix elements for natural parity (electric), and unnatural parity (magnetic) transitions, are given in Ref. [21].

### 3 Details of the calculations

We have applied the formalism described in the previous section to calculate the excitation spectrum of single  $\Lambda$  hypernuclei formed by the excitation of nucleonic doubly closed shell nuclei. Specifically, we have investigated the  ${}_{\Lambda}^{12}\text{C}$ ,  ${}_{\Lambda}^{16}\text{O}$ ,  ${}_{\Lambda}^{40}\text{Ca}$ ,  ${}_{\Lambda}^{90}\text{Zr}$  and  ${}_{\Lambda}^{208}\text{Pb}$  hypernuclei.

		$c$	$\sigma$	$t$
LN $\delta$		20.0	70.0	-28.0
	$w_1$	-4.5	-1.26	15.0
LND	$w_2$	-104.0	-7.56	145.0
	$w_3$	590.0	182.0	1.0
	$w_1$	0.0	-1.0	8.0
LNDE	$w_2$	-92.0	-3.5	50.0
	$w_3$	518.0	90.0	100.0
	$\beta_1$	1.5	1.5	1.0
	$\beta_2$	0.9	0.9	0.6
	$\beta_3$	0.5	0.5	0.4

Table 1: Values of the parameters of the three  $\Lambda$ -nucleon interactions used in this work. The LN $\delta$  interaction is of zero range type, and, in the table, we indicate the values of the  $U^{c,\sigma,t}$  parameters of Eq. (32) in MeV fm<sup>3</sup>. The other two interactions have been constructed as indicated by Eqs. (33) and (34). The values of the  $w$  coefficients for the scalar ( $c$ ) and spin ( $\sigma$ ) channels are expressed in MeV, those of the tensor channel ( $t$ ) in MeV fm<sup>-2</sup>. The ranges of the gaussians  $\beta_i$  are the same for both LND and LNDE interactions and their values are expressed in fm.

		${}_{\Lambda}^{16}\text{O}$				
$J^\pi$	p h	MF	LN $\delta$	LND	LNDE	exp
$0^-$	$(1s_{1/2})_{\Lambda}(1p_{1/2})_n^{-1}$	0.0	0.0	0.0	0.0	0.0 [33]
$1_1^-$	$(1s_{1/2})_{\Lambda}(1p_{1/2})_n^{-1}$	0.0	0.71	0.71	0.69	0.026 [32]
$1_2^-$	$(1s_{1/2})_{\Lambda}(1p_{3/2})_n^{-1}$	6.16	6.58	6.55	6.56	6.562 [33]
$2^-$	$(1s_{1/2})_{\Lambda}(1p_{3/2})_n^{-1}$	6.16	6.77	6.76	6.79	6.784 [33]
$1^+$	$(1p_{3/2})_{\Lambda}(1p_{1/2})_n^{-1}$	9.97	10.25	10.10	10.36	
$2^+$	$(1p_{3/2})_{\Lambda}(1p_{1/2})_n^{-1}$	9.97	10.33	10.39	10.43	10.57 [31]
$0^+$	$(1p_{1/2})_{\Lambda}(1p_{1/2})_n^{-1}$	11.17	11.10	10.40	10.55	

Table 2: Energies in MeV of the  ${}_{\Lambda}^{16}\text{O}$  spectrum, obtained in MF approximation, and with the three interactions used in our work, compared to the experimental values given in Refs. [32, 33, 31]. The energy resolution obtained in [32, 33] is of few keV, while that of the  $2^+$  state is of 2 MeV [31]. The MF particle-hole components are also shown.

In analogy to what is done in the application of the Landau-Migdal theory [22] to finite nuclear systems [23, 24], the mean field is described by a phenomenological potential, in our case a spherical Woods-Saxon well, of the form

$$\begin{aligned}
 U^t(r) &= \frac{-V_0^t}{1 + \exp\left[\left(r - R_0^t\right)/a_0^t\right]} \\
 &- \left[\frac{\hbar c}{m_\pi c^2}\right]^2 \left(\frac{V_{ls}^t}{a_{ls}^t r}\right) \frac{\exp\left[\left(r - R_{ls}^t\right)/a_{ls}^t\right]}{\left\{1 + \exp\left[\left(r - R_{ls}^t\right)/a_{ls}^t\right]\right\}^2} \mathbf{1} \cdot \boldsymbol{\sigma} - V_C^t(r), \quad (30)
 \end{aligned}$$

where  $m_\pi$  is the pion mass and the Coulomb term  $V_C^t(r)$ , active only for protons, is that produced by a homogeneous charge distribution.

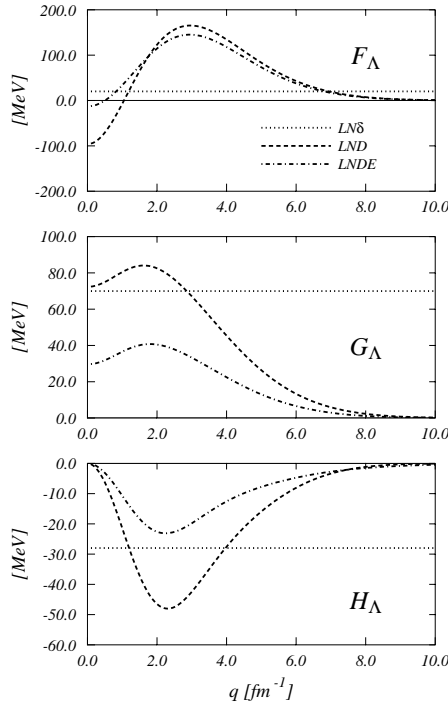


Figure 1: Momentum dependence of the  $\Lambda$ - nucleon interactions for each channel of Eq. (19). The  $LN\delta$  zero-range interaction is constant in momentum space. The parameters of the other two interactions are given in Tab. 1.

For the nucleonic part we used parameterizations chosen to reproduce the single particle energies of the levels close to the Fermi surface and the r.m.s. charge radii. The parameters of these potentials have been taken from the literature [25] for the  $^{12}\text{C}$ ,  $^{16}\text{O}$ ,  $^{40}\text{Ca}$  and  $^{208}\text{Pb}$  nuclei. For the  $^{90}\text{Zr}$  nucleus we used  $V_0^p=55.88$  MeV,  $V_0^n=48.12$  MeV,  $V_{ls}^p = V_{ls}^n=7.7$  MeV, and  $a_0^{p,n} = a_{ls}^{p,n}=0.645$  fm, and  $R_0^{p,n}=5.695$  fm,  $R_{ls}^{p,n}=5.68$  fm.

In our calculations also the  $\Lambda$  mean field potential is described by a spherical Woods-Saxon well with a set of parameters values very close to those given in [26]. We used  $V_0^\Lambda=29.0$  MeV,  $V_{ls}^\Lambda=2.0$  MeV, and  $a_0^\Lambda = a_{ls}^\Lambda=0.6$  fm for all the hypernuclei, and we changed the radii in order to reproduce the ground state binding energies of the various hypernuclei. For  $^{12}_\Lambda\text{C}$ ,  $^{16}_\Lambda\text{O}$ ,  $^{40}_\Lambda\text{Ca}$ ,  $^{90}_\Lambda\text{Zr}$  and  $^{208}_\Lambda\text{Pb}$  we used  $R_0^\Lambda = R_{ls}^\Lambda=2.50, 2.73, 4.00, 5.60, 7.60$  fm, respectively.

In both the nucleonic and  $\Lambda$  sectors the mean-field potential is diagonalized in a truncated harmonic oscillator basis. This procedure discretizes automatically the continuum. Since we are interested in the lowest excited states a proper description of the escape width is not necessary [23]. In Sect. 4 we discuss results obtained for excited states dominated by particle-hole transitions where the  $\Lambda$  is in a bound state.

Our calculations have been done with a configuration space which considers 54 single particle levels describing the  $\Lambda$  hyperon, up to the  $5p_{1/2}$  level. This corresponds to consider 10 major harmonic oscillator shells. A comparison with results obtained with a smaller configuration space of only 22 states, up to the  $3p_{1/2}$  level, shows differences in the eigenvalues of about 10, 20 keV.

As already indicated in Eq. (19), the residual interaction between  $\Lambda$  and the nucleons is considered

to be a sum of scalar, spin and tensor terms

$$V_{\Lambda N} = V_{\Lambda N}^c(r) + V_{\Lambda N}^\sigma(r) \boldsymbol{\sigma}(\Lambda) \cdot \boldsymbol{\sigma}(N) + V_{\Lambda N}^t(r) \left[ 3 \frac{(\boldsymbol{\sigma}(\Lambda) \cdot \mathbf{r})(\boldsymbol{\sigma}(N) \cdot \mathbf{r})}{r^2} - \boldsymbol{\sigma}(\Lambda) \cdot \boldsymbol{\sigma}(N) \right]. \quad (31)$$

In the above equation  $N$  indicates the nucleon and the  $V_{\Lambda N}^{c,\sigma,t}(r)$  terms are the Fourier transforms of the  $F_\Lambda$ ,  $G_\Lambda$  and  $H_\Lambda$  terms of Eq. (19). With respect to the  $\Lambda$ -nucleon interactions commonly used in shell-model calculations [11], we neglect the spin-orbit term. The contribution of this term is rather small [27], and we consider it at the mean-field level by including a spin-orbit term in the Woods-Saxon potentials. The effects of the spin-orbit terms of the residual interaction have been studied in self-consistent RPA calculations for ordinary nuclei [28] and they have been found to be rather small.

The sensitivity of our results to the  $\Lambda$ -nucleon interaction has been tested by comparing the results obtained with three different parameterizations of the  $V_{\Lambda N}^{c,\sigma,t}(r)$  functions. In a first parameterization, which we call LN $\delta$ , the three functions are assumed to be of zero-range type

$$V_{\Lambda N}^{c,\sigma,t}(r) = U_{\Lambda N}^{c,\sigma,t} \delta(r). \quad (32)$$

The values of the constants  $U^{c,\sigma,t}$  are given in the first row of Tab. 1.

For the other two interactions, in analogy to the YNG interaction [29, 30], we parametrize each radial term of the force (31) as a sum of three gaussians, specifically,

$$V_{\Lambda N}^{c,\sigma}(r) = \sum_{i=1,3} w_i^{c,\sigma} \exp[-(r/\beta_i^{c,\sigma})^2], \quad (33)$$

for the scalar and spin terms, and

$$V_{\Lambda N}^t(r) = \sum_{i=1,3} w_i^t r^2 \exp[-(r/\beta_i^t)^2], \quad (34)$$

for the tensor term.

The interaction LN $\delta$  and the finite range interaction LND are used in calculations where only the direct terms of the interaction matrix elements, see Eq. (16), are considered, while we consider both direct and exchange terms when we use the finite range interaction we call LNDE. The values of the parameters of each interaction have been chosen to reproduce at best the energies of the first  $0^-$ ,  $2^-$  and  $1^-$  excited states of  ${}^{16}_\Lambda\text{O}$ . These parameters values are given in Tab. 1 and the momentum dependence of the three interactions is shown in Fig. 1. In Tab. 2, we compare the results of our calculations in  ${}^{16}_\Lambda\text{O}$  with the experimental values presented in Refs. [31, 32, 33]. In the table all the energies have been renormalized to the energy of the lowest state, which, in our calculations, is always the  $0^-$ .

We have also calculated the spectrum of  ${}^{16}_\Lambda\text{O}$  with the YNG interaction of Refs. [29, 30]. This force reproduces the G-matrix interaction built on a Nijmegen  $\Lambda$ -nucleon potential [34]. The spectrum we have obtained with this interaction, is rather different from the experimental one. The lowest energy state is a  $1^+$  followed by a  $1^-$  at 0.49 MeV, a  $2^-$  at 13.34 MeV. The first  $0^-$  state appears at 17.94 MeV. We expected such a bad result, since our theory requires interactions which effectively consider also many-body effects not included in the G-matrix calculations [35]. For this reason a straightforward comparison between our effective interactions with more microscopic interactions is not appropriate.

## 4 Results

Before presenting the results obtained by applying our model to  ${}^{12}_\Lambda\text{C}$ ,  ${}^{16}_\Lambda\text{O}$ ,  ${}^{40}_\Lambda\text{Ca}$ ,  ${}^{90}_\Lambda\text{Zr}$  and  ${}^{208}_\Lambda\text{Pb}$  hypernuclei, we make a comment about the presence of some ground state correlations in our model. In our approach, these correlations are taken into account by the  $Z$  amplitudes. These effects are related to the RPA-like description of the ground state [15], and they describe a limited set of correlations. For example

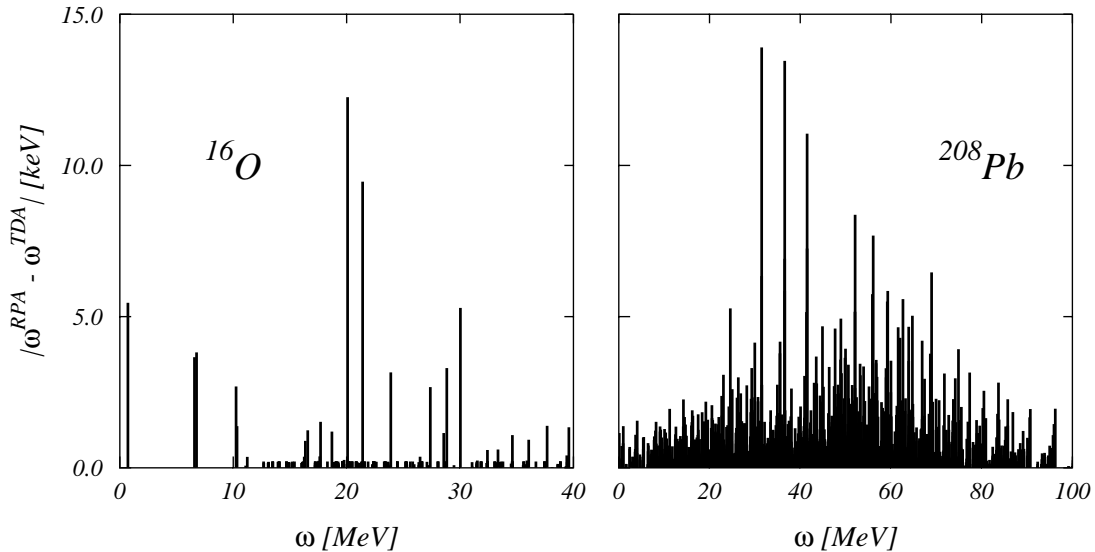


Figure 2: Differences between RPA-like and TDA energy eigenvalues of  ${}_{\Lambda}^{16}\text{O}$  and  ${}_{\Lambda}^{208}\text{Pb}$  hypernuclei calculated with the LN $\delta$  interaction.

they do not describe the short-range correlations [36], and they do not consider the partial occupation probability of single particle states both below and above the Fermi surface. We have already pointed out that in our model nucleonic correlations are not considered.

A quantitative indication of the relevance of these RPA-like ground state correlations, can be obtained by comparing our results with those of the TDA theory obtained by solving Eq. (7) without the term which multiplies the  $Z$  amplitude. Since we work with a discrete configuration space, the number of eigenstates corresponding to positive energies obtained in RPA and TDA is the same. For this reason we can immediately identify the energy difference of each eigenstate. As an example of the results we have obtained, we show in Fig. 2 these energy differences for the  ${}_{\Lambda}^{16}\text{O}$  and  ${}_{\Lambda}^{208}\text{Pb}$  hypernuclei as a function of the RPA energy. These results have been obtained by using the LN $\delta$  interaction. In the left panel of the figure we show 273  ${}_{\Lambda}^{16}\text{O}$  energy differences corresponding to all the solutions we found for all the positive and negative parity multipole excitations up to  $J = 4$ . In the case of  ${}_{\Lambda}^{208}\text{Pb}$  we show 5024 energies differences corresponding to multipole excitations up to  $J = 10$ .

We observe that only in few cases the energy differences are larger than 10 keV. Specifically, for the states of our interest, below 10 MeV for  ${}_{\Lambda}^{16}\text{O}$  and below 4 MeV for  ${}_{\Lambda}^{208}\text{Pb}$ , these differences are even smaller. The results of our RPA-like theory and those of the TDA are quantitatively equivalent. However, since the RPA is the complete and consistent theory describing linear combination of one-particle, one-hole excitations [15], we used our RPA-like model to obtain all the results presented in the remaining part of the article.

We start the presentation of our results by showing in Tab. 2 the spectrum of  ${}_{\Lambda}^{16}\text{O}$ . In this table also the MF results and the experimental values of Refs. [31, 32, 33] are shown. The energy differences between the  $0^-$ ,  $2^-$  and  $1_2^-$  states have been used to adjust the parameters of the  $\Lambda$ -nucleon forces. These parameterizations are not unique. We have found sets of parameters values which produce very collective  $0^+$  states at low energy, in some case this was even the lowest energy state. While there are no experimental evidences of such low energy  $0^+$  state, there are indications of a  $0^+$  state around 10-11 MeV [37, 38]. For this reason we have used forces predicting a  $0^+$  state around 11 MeV. The energies of the other states are a prediction of our model.

The MF energies are already rather close to the experimental values and our RPA-like results change

$^{16}_{\Lambda}O$

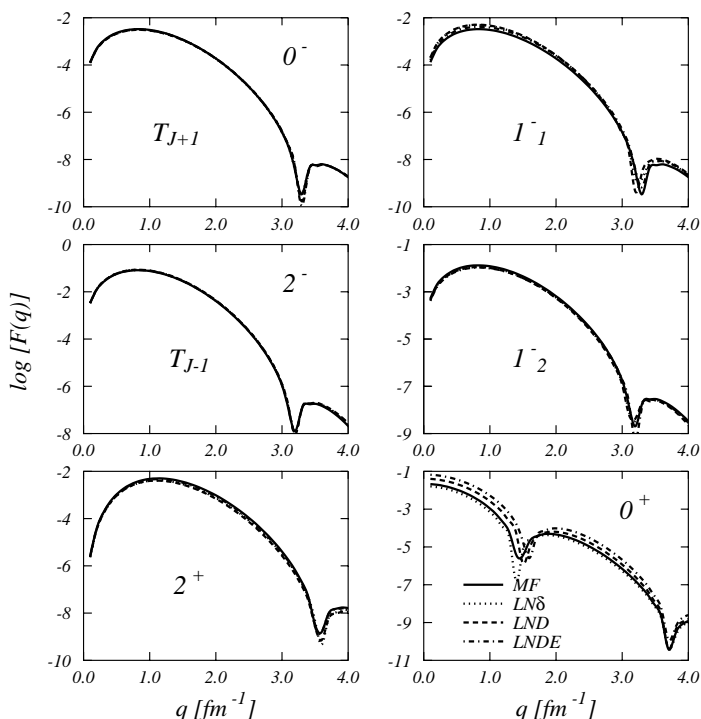


Figure 3: Transition form factors, Eq. (35), obtained in MF approximation and calculated with the three residual interactions used in this work, as a function of the momentum  $q$  of the operators (21) and (24). For the unnatural parity excitations  $0^-$  and  $2^-$ , the operator inducing the transition is indicated, see Eq. (24). The subindexes 1 and 2 of the  $1^-$  states indicate the lower and higher energies states respectively, see Tab. 2.

them by about 4% on average. The experimental splitting between the two  $1^-$  states is not well reproduced. Better agreement could be obtained with a rearrangement of the force parameters, or by including additional force terms such as the spin-orbit or velocity dependent terms.

The structure of the  $0^+$  state is somehow more collective than those of the other states of the spectrum. This feature becomes more evident by observing the transition matrix elements from the ground state to the hypernuclear excited states. In Fig. 3 we show the transition form factors

$$F(q) = |\langle \Psi_0 | T(q) | \Psi_\nu \rangle|^2, \quad (35)$$

for the negative parity states of the spectrum and for the  $0^+$  and the  $2^+$  states. The transition operators are defined in Eqs. (21) and (24) for natural and unnatural parity states respectively. For unnatural parity excitations, we use transition operators characterized by  $L = J \pm 1$ . In the case of the  $0^-$  state only the  $T_{J+1}$  is active, while for the  $2^-$ , both operators are active. In this last case, however, we found that the  $T_{J+1}$  form factor is zero in mean-field approximation, and four orders of magnitudes smaller than the  $T_{J-1}$  form factor when the residual interaction is active. For this reason we neglect it in our discussion. In Fig. 3 the transition form factors for the two  $1^-$  states are labeled with the subindexes 1 and 2 to indicate the lower and higher energy states respectively, see Tab. 2. Finally, in the lower panels we show the transition form factors for the  $2^+$  and  $0^+$  states.

The behavior of these form factors as a function of  $q$  is rather interesting. Only the  $0^+$  transition shows a maximum at values of  $q$  near zero. For this reason substitutional experiments such as ( $K^-$ ,  $\pi^-$ )

${}_{\Lambda}^{16}\text{O}$					
	MF	LN $\delta$	LND	LNDE	[39]
M1 ( $1_1^- \rightarrow 0^-$ )	0.0	0.081	0.082	0.083	0.176
M1 ( $1_2^- \rightarrow 0^-$ )	0.433	0.406	0.406	0.404	0.336
M1 ( $1_2^- \rightarrow 1_1^-$ )	0.217	0.248	0.248	0.250	0.129
M1 ( $2^- \rightarrow 1_1^-$ )	0.650	0.680	0.680	0.683	
M1 ( $2^- \rightarrow 1_2^-$ )	0.0	0.050	0.049	0.048	
E1 ( $0^+ \rightarrow 1_1^-$ )	0.231	0.232	0.309	0.329	
E1 ( $0^+ \rightarrow 1_2^-$ )	0.0	0.012	0.002	0.006	

Table 3: Electromagnetic transitions between various states of  ${}_{\Lambda}^{16}\text{O}$ , in Weisskopf units, compared to the shell model results of Ref. [39].

are better suited to investigate the  $0^+$  states than experiments which produce hypernuclei with a rather large value of the momentum transfer, such as  $(e, e'K^+)$  [30].

In Fig. 3 the MF transition form factors are compared with those obtained in our RPA-like calculations with the three interactions. For the cases we have investigated, we have found that the presence of the interaction does not modify sensitively the MF results, but for the  $0^+$  state. In this last case, while the LN $\delta$  result is similar to the MF one, the two finite-range interactions produce rather different form factors. In the MF model the particle-hole excitation generating the lowest  $0^+$  state is the  $(1p_{1/2})_{\Lambda}(1p_{1/2})_n^{-1}$  transition. This is also the main transition ( $W=0.998$ ) obtained in the calculation with the LN $\delta$  interaction. The situation changes slightly when the LND interaction is used, since a relevant contribution of the  $(1p_{3/2})_{\Lambda}(1p_{3/2})_n^{-1}$  transition ( $W = 0.121$ ) is associated to the still dominant  $(1p_{1/2})_{\Lambda}(1p_{1/2})_n^{-1}$  transition ( $W=0.987$ ). The calculation with the LNDE interaction produces a  $0^+$  state with a rather different structure. The main transition is now the  $(1p_{3/2})_{\Lambda}(1p_{3/2})_n^{-1}$  ( $W=0.843$ ) with a large contribution of the  $(1p_{1/2})_{\Lambda}(1p_{1/2})_n^{-1}$  component ( $W=0.366$ ) and also of the  $(1s_{1/2})_{\Lambda}(1s_{1/2})_n^{-1}$  component ( $W=-0.327$ ).

We obtain another indication of the relative collectivity of the  $0^+$  state by studying the electromagnetic transitions between the excited states of  ${}_{\Lambda}^{16}\text{O}$ . The B-values of these transitions are shown in Tab. 3. The transitions forbidden in MF calculations have relatively small values when the residual interaction is switched on. All the M1 transitions are modified on the second significant figure by the residual interaction. We use three digits to show the difference between the results obtained with the various interactions. The situation changes when the  $0^+$  state is present. The B-values of the  $(0^+ \rightarrow 1_1^-)$  transition are quite different in the various calculations. The LN $\delta$  result is similar to that obtained in MF approximation, while the values obtained with the LND and LNDE interactions are 38% and 48% larger than the MF value. This result is again a consequence of the collective structure of the  $0^+$  state.

In Tab. 3 we compare some of our results with those obtained in shell model calculations [39]. The order of magnitude of the B-values is the same in the two calculations, but the differences are remarkable. Our results are roughly a factor two smaller for the  $1_1^- \rightarrow 0^-$  transition and a factor two larger for the  $1_2^- \rightarrow 1_1^-$  transition. The difference between the results for the other transition is 17%. It would be interesting to compare with experimental values. Unfortunately, while the experimental identification of the energies of the spectrum is quite accurate [40], the measure of the B-values of the transition requires higher statistics. The technological improvements are very promising and these measurements will become feasible in the near future.

In Tab. 4 we compare the  ${}_{\Lambda}^{12}\text{C}$  spectrum with the energies measured in the E369 [4] and FINUDA [6] experiments. The uncertainty in the energy resolution of the E369 experiment is about 1.5 MeV, and that of the FINUDA experiment is 1.29 MeV. The angular momentum and parity assignment to the energies measured in the FINUDA experiment is our guess.

The presence in the experimental spectrum of two  $1^-$  states, that we have called  $1_{2,3}^-$ , is not predicted by our model. Shell model calculations [41, 42] indicate that these states are produced by neutron- $\Lambda$  transitions where the neutron is in the  $1p_{1/2}$  state, above the Fermi surface in the MF model. The

		${}_{\Lambda}^{12}\text{C}$					
$J^{\pi}$	p h	MF	LN $\delta$	LND	LNDE	E369	FINUDA
$1_1^-$	$(1s_{1/2})_{\Lambda}(1p_{3/2})_n^{-1}$	0.0	0.0	0.0	0.0	0.0	0.0
$2^-$	$(1s_{1/2})_{\Lambda}(1p_{3/2})_n^{-1}$	0.0	0.26	0.24	0.27	-	-
$1_2^-$		-	-	-	-	2.63	2.54
$1_3^-$		-	-	-	-	6.09	5.04
$0^+$	$(1p_{3/2})_{\Lambda}(1p_{3/2})_n^{-1}$	10.03	9.61	8.39	8.28	8.12	7.14
$2^+$	$(1p_{3/2})_{\Lambda}(1p_{3/2})_n^{-1}$	10.03	9.38	9.33	9.79	-	9.34
$1^+$	$(1p_{3/2})_{\Lambda}(1p_{3/2})_n^{-1}$	10.03	9.69	9.58	9.94	11.00	11.21
$3^+$	$(1p_{3/2})_{\Lambda}(1p_{3/2})_n^{-1}$	10.03	9.87	9.80	9.95	-	-

Table 4: Energies in MeV of the  ${}_{\Lambda}^{12}\text{C}$  spectrum calculated in MF approximation and with the three interactions used in our work. The experimental values of E369 [4] are those reported in [11]. The values of the FINUDA experiment [6] have been rescaled with respect to the lowest energy value, and the angular momentum and parity assignment is our guess. The uncertainty in the energy resolution of the E369 experiment is 1.45 MeV, and that of the FINUDA experiment of 1.29 MeV. The MF particle-hole transitions are also shown.

ground state correlations of our approach do not consider partial occupation probability of the single particle levels, therefore we are unable to predict these excitations. A description of  ${}^{12}\text{C}$  as closed shell nucleus is reasonable in kinematic regions where the detailed shell structure is not relevant, such as giant resonances or the quasi-elastic region, but for the case we are treating it is inadequate.

		${}_{\Lambda}^{12}\text{C}$				
		MF	LN $\delta$	LND	LNDE	[43]
M1	$(2^- \rightarrow 1_1^-)$	0.0	0.082	0.082	0.082	-
E1	$(0^+ \rightarrow 1_1^-)$	0.278	0.246	0.421	0.509	0.475
E1	$(2^+ \rightarrow 1_1^-)$	0.139	0.135	0.121	0.158	0.133
E1	$(2^+ \rightarrow 2^-)$	0.139	0.170	0.194	0.133	0.094

Table 5: Electromagnetic transitions between various states of  ${}_{\Lambda}^{12}\text{C}$ , in Weisskopf units, compared with the shell model results of Ref. [43].

Our model predicts the presence of excited states between 8 and 11 MeV. These states are all coming from the  $(1p_{3/2})_{\Lambda}(1p_{3/2})_n^{-1}$  excitation, and in MF approximation are degenerate at 10.03 MeV. The residual interaction removes this degeneracy, and, in general, the excitation energy of each state is lowered with respect to the MF value. The  $0^+$  and  $2^+$  states are the lowest ones. The LND and LNDE interactions give the  $0^+$  around 8.5 MeV, where E369 finds a peak. The identification of this experimental peak with our  $0^+$  is however quite dubious, since the experiment produces hypernuclei by using a probe that transfers high momentum values to the system, while the  $0^+$  response has its maximum at small  $q$  values. This is shown in the lowest right panel of Fig. 4, where the transition form factor of this  $0^+$  state is shown.

In our search for collective effects we have studied the transition form factors of the various excitations, and, in Fig. 4, we show some of them. This figure is analogous to Fig. 3, but for  ${}_{\Lambda}^{12}\text{C}$ . We have selected the transition form factors of the positive states degenerate in MF, and the lowest  $1^-$  state. For the  $3^+$  state we show only the  $T_{J-1}$  form factor, since the  $T_{J+1}$  is zero in the MF model.

The figure shows that the  $2^+$  and  $3^+$  transitions are essentially unaffected by the effective interaction, as it is the ground state  $1^-$  transition. The  $0^+$  state, and, much more, the  $1^+$  state, are instead rather sensitive to the presence of the residual interaction. The structure of the  $1^+$  state is not collective. In our calculation this state is described by the combination of two particle-hole transitions, the  $(1p_{3/2})_{\Lambda}(1p_{3/2})_n^{-1}$  transitions, which is the dominant one, and the  $(1p_{1/2})_{\Lambda}(1p_{3/2})_n^{-1}$  transition. While in MF approximation this state is described only by the first transition, the relative weight of the two

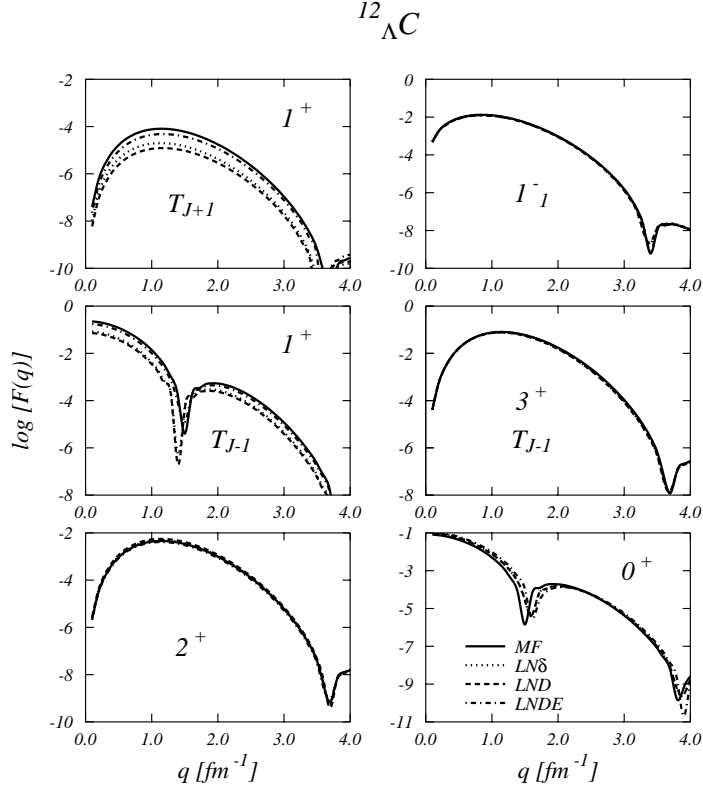


Figure 4: Transition form factors as in Fig. 3, but for  $^{12}_{\Lambda}C$ . The energies of the various excited states are given in Tab. 4.

particle-hole components changes with the residual interaction. The values of the  $W$  amplitudes vary, respectively, from 0.99 and 0.10 for the LNDE interaction to 0.94 and 0.33 for LN $\delta$ . These different couplings between the two states are sufficient to produce the spreading of the form factors shown in Fig. 4.

Also the RPA-like structure of the  $0^+$  state is mostly described by the combination of the  $(1p_{3/2})_{\Lambda}(1p_{3/2})_n^{-1}$  and  $(1s_{1/2})_{\Lambda}(1s_{1/2})_n^{-1}$  transitions. These are the only two relevant transitions in the formation of the  $0^+$  state. The relative weights of these two transitions change by changing the residual interaction, and this produces the spreading of the form factors shown in Fig. 4.

The B-values of some of the  $\gamma$  transitions for the  $^{12}_{\Lambda}C$  hypernucleus are shown in Tab. 5, and they are compared with the shell model results of Ref. [43]. The  $2^- \rightarrow 1^-$  M1 transition is not present in the MF model, since the two states are degenerate. Our RPA-like calculations remove this degeneracy and produce B-values which are almost insensitive to the different residual interactions.

The B-values of the E1 transitions  $2^+ \rightarrow 1^-$  and  $2^+ \rightarrow 2^-$  obtained in the MF model are identical, since the wave functions of the initial and final states are the same, as it can be deduced from the MF transitions shown in Tab. 4. The B-values obtained in our RPA-like calculations are rather similar to the MF values. The situation changes for the  $0^+ \rightarrow 1^-$  E1 transition, where our RPA-like results modify the MF value by 10, 70 and 100% when the LN $\delta$ , LND and LNDE interactions are used, respectively. As for  $^{16}_{\Lambda}O$ , also in this case the structure of the  $0^+$  state is extremely sensitive to the residual interaction. In our model this state is described by a combination of the  $(1p_{3/2})_{\Lambda}(1p_{3/2})_n^{-1}$  transition, the dominant one, and the  $(1s_{1/2})_{\Lambda}(1s_{1/2})_n^{-1}$  transition. The coefficients of these two particle-hole transitions are changed by the residual interaction and this produces the changes in the B-values. The agreement between our

results with those of the shell model [43] is more satisfactory than in the case of the  $^{16}_{\Lambda}\text{O}$  hypernucleus.

In Tab. 6 we show the results relative to the spectrum of the  $^{40}_{\Lambda}\text{Ca}$  hypernucleus, for energies smaller than 10 MeV. The changes of the RPA-like energies, with respect to those of the MF calculations, are 3.5%, on average. The only exception is the  $1_2^+$  state which shows changes around 20 %. We have analyzed the transition form factors of this state, but we did not find any remarkable effect which distinguishes it from the MF result.

$^{40}_{\Lambda}\text{Ca}$						
$J^\pi$	p h	MF	LN $\delta$	LND	LNDE	[44]
$1_1^+$	$(1s_{1/2})_{\Lambda}(1d_{3/2})_n^{-1}$	0.0	0.0	0.0	0.0	0.22
$2_1^+$	$(1s_{1/2})_{\Lambda}(1d_{3/2})_n^{-1}$	0.0	0.16	0.21	0.19	0.0
$0^+$	$(1s_{1/2})_{\Lambda}(2s_{1/2})_n^{-1}$	2.60	2.50	2.74	2.42	2.92
$1_2^+$	$(1s_{1/2})_{\Lambda}(2s_{1/2})_n^{-1}$	2.60	3.07	3.13	2.93	3.44
$2_2^+$	$(1s_{1/2})_{\Lambda}(1d_{5/2})_n^{-1}$	6.00	6.04	6.08	6.09	6.19
$3^+$	$(1s_{1/2})_{\Lambda}(1d_{5/2})_n^{-1}$	6.00	6.10	6.10	6.11	6.01
$2_1^-$	$(1p_{3/2})_{\Lambda}(1d_{3/2})_n^{-1}$	7.81	7.72	7.69	7.77	7.98
$0^-$	$(1p_{3/2})_{\Lambda}(1d_{3/2})_n^{-1}$	7.81	7.77	8.02	7.07	9.54
$1_1^-$	$(1p_{3/2})_{\Lambda}(1d_{3/2})_n^{-1}$	7.81	7.95	7.91	8.05	8.78
$3^-$	$(1p_{3/2})_{\Lambda}(1d_{3/2})_n^{-1}$	7.81	8.04	8.24	7.99	8.55
$2_2^-$	$(1p_{1/2})_{\Lambda}(1d_{3/2})_n^{-1}$	8.58	8.61	8.59	8.59	9.53
$1_2^-$	$(1p_{1/2})_{\Lambda}(1d_{3/2})_n^{-1}$	8.58	8.74	8.51	8.36	9.27

Table 6: Energies in MeV of the  $^{40}_{\Lambda}\text{Ca}$  spectrum calculated in MF approximation and with the three interactions used in our work. Our results are compared with the shell model results of Ref. [44]. We have considered all the states with energy smaller than 10 MeV. The MF particle-hole transitions are shown.

We observe in Tab. 6 that, in our calculations, the ground state of the  $^{40}_{\Lambda}\text{Ca}$  system is produced by the  $(1s_{1/2})_{\Lambda}(1d_{3/2})_n^{-1}$  transition which in MF approximation gives two degenerate states characterized by angular momenta and parity  $1^+$  and  $2^+$ . All our RPA-like calculations remove the degeneracy by lowering the  $1^+$  state, while it is the opposite in the calculation of Ref. [44]. In general, the comparison between our results and those of Ref. [44] shows an agreement in terms of clustering of states around the MF single-particle transitions. However, within the set of states produced by the same MF transition, there are some inversions of the multipoles. This happens for the MF degenerate  $2_2^+$  and  $3^+$  states, as well as for the set of degenerate states produced by the  $(1p_{3/2})_{\Lambda}(1d_{3/2})_n^{-1}$  transition and also for the  $(1p_{1/2})_{\Lambda}(1d_{3/2})_n^{-1}$  transition. A measure of the experimental spectrum of  $^{40}_{\Lambda}\text{Ca}$  would clarify the situation.

$^{90}_{\Lambda}\text{Zr}$					
p	MF	LN $\delta$	LND	LNDE	exp [4]
$(1s_{1/2})_{\Lambda}$	0.0	$0.003 \pm 0.003$	$0.005 \pm 0.009$	$0.007 \pm 0.012$	0.0
$(1p_{1/2})_{\Lambda}$	4.994	$5.012 \pm 0.061$	$5.010 \pm 0.058$	$4.999 \pm 0.031$	4.9
$(1d_{5/2})_{\Lambda}$	10.749	$10.783 \pm 0.077$	$10.766 \pm 0.060$	$10.743 \pm 0.038$	11.5
$(1f_{7/2})_{\Lambda}$	16.994	$17.016 \pm 0.035$	$17.013 \pm 0.039$	$17.002 \pm 0.029$	19.0

Table 7: Energies, in MeV, of the various states coupled to the  $1g_{9/2}$  neutron hole in  $^{90}_{\Lambda}\text{Zr}$ , calculated in MF and in our RPA-like approach for the three  $\Lambda$ -nucleon interactions used in this work. The energies of the RPA-like results are the averages of the various excitation energies of each multipole excitation compatible with the indicated single particle transition. The experimental energies are those of the  $^{89}_{\Lambda}\text{Y}$  hypernucleus, and the uncertainty in the determination of the energy is roughly 1 MeV.

We have studied the spectra of the  $^{90}_{\Lambda}\text{Zr}$  and  $^{208}_{\Lambda}\text{Pb}$  hypernuclei and we have observed that also in

these cases the changes with respect to the MF results are rather small, about 100 keV, of the order of the 2, maximum 3% on average.

As an example of our results, we show in Tab. 7 the energies of the excited states of  ${}_{\Lambda}^{90}\text{Zr}$  obtained by considering the transitions of the  $1g_{9/2}$  neutron hole to the  $\Lambda$  single particle states. This MF picture has been used in the analysis of the  $(\pi^+, K^+)$  reaction on  ${}_{\Lambda}^{89}\text{Y}$  target [4]. In the same spirit, we have studied the excitation of this neutron hole into the  $s, p, d, f$  states of the  $\Lambda$  with  $j_{\Lambda} = l_{\Lambda} + 1/2$ . We have considered all the possible multipole excitations compatible with a specific neutron- $\Lambda$  transition. Obviously, in the MF calculation all these states have the same excitation energy. Our RPA-like calculations, however, give different energy values for each multipole excitation. In Tab. 7 we compare the MF energies for each transition with our RPA-like energies obtained by averaging the results of the various multipole excitations, and we also show their standard deviation. We observe that, within the statistical uncertainty, RPA-like and MF results coincide. Also the agreement with the experimental values is good, especially if we consider that the data are taken on a  ${}_{\Lambda}^{89}\text{Y}$  target, and they have an uncertainty of  $1.65 \pm 0.10$  MeV.

${}_{\Lambda}^{208}\text{Pb}$						
p	MF	LN $\delta$	LND	LNDE	exp1	exp2
$(1s_{1/2})_{\Lambda}$	1.633	$1.630 \pm 0.001$	$1.629 \pm 0.002$	$1.623 \pm 0.008$	1.6	-3.0
$(1p_{1/2})_{\Lambda}$	4.621	$4.629 \pm 0.024$	$4.626 \pm 0.025$	$4.616 \pm 0.016$	6.8	4.6
$(1d_{5/2})_{\Lambda}$	8.220	$8.237 \pm 0.036$	$8.230 \pm 0.030$	$8.216 \pm 0.017$	12.84	8.24
$(1f_{7/2})_{\Lambda}$	12.344	$12.354 \pm 0.020$	$12.345 \pm 0.010$	$12.328 \pm 0.014$	18.29	13.69
$(1g_{9/2})_{\Lambda}$	16.926	$16.948 \pm 0.034$	$16.959 \pm 0.040$	$16.926 \pm 0.108$	22.10	17.49

Table 8: Energies, in MeV, of the various states coupled to the  $1i_{13/2}$  neutron hole in  ${}_{\Lambda}^{208}\text{Pb}$ , calculated in MF and in our RPA-like approach for the three  $\Lambda$ -nucleon interactions used in our work. The energies of the RPA-like results are the averages of the various excitation energies of each multipole excitation compatible with the indicated single particle transition. The values shown in the columns exp1 and exp2 are the experimental energies of Ref. [2], rescaled in two different manners (see text).

The results of an analogous study for the  $1i_{13/2}$  neutron hole in  ${}_{\Lambda}^{208}\text{Pb}$  coupled with the  $s, p, d, f, g$  states of the  $\Lambda$  with  $j_{\Lambda} = l_{\Lambda} + 1/2$ , are shown in Tab. 8. The RPA-like energies are all compatible with the MF ones, within the statistical uncertainty. In the same table we compare our results with the energies given in Ref. [2] where the  $(\pi^+, K^+)$  scattering data on a  ${}^{208}\text{Pb}$  target have been analyzed in terms of transitions of the  $1i_{13/2}$  neutron hole. Since, in our calculations, the lowest energy of  ${}_{\Lambda}^{208}\text{Pb}$  is produced by the transition  $(1s_{1/2})_{\Lambda}(3p_{1/2})_n^{-1}$ , we have positioned the first experimental energy of Ref. [2] at 1.63 MeV, which is the difference between the  $3p_{1/2}$  and  $1i_{13/2}$  neutron single particle energies. The other energies have been consistently rescaled, and their values are shown in Tab. 8 by the column labeled exp1. The agreement is not satisfactory even if we consider that the experimental energy resolution is of  $2.2 \pm 0.1$  MeV. We then set the position of the second experimental energy at 4.6 MeV, to match our second state, and we rescale the other energies. The corresponding values are shown in the column exp2. In this case the agreement with our results noticeably improves. The source of disagreement with our results is in the energy difference between the first two states.

Up to now, we have presented our results by considering individually each hypernucleus. To give a more general view, we show in Fig. 5 the density of states of the various hypernuclei as a function of the excitation energy. The different lines indicate the results obtained in MF and RPA-like approaches by using the various residual interactions. In our model, the number of excited states for a given multipolarity depends only on the configuration space, and not on the residual interaction. For this reason, differences between the lines of each panel of the figure indicate the relevance of the  $\Lambda$ -nucleon residual interaction which shifts the excitation energies with respect to the MF results. For each hypernucleus, we have taken into account all the possible multipole excitations which provide a solution below 20 MeV.

A first remark on the results shown in Fig. 5 is that the density of states in  ${}_{\Lambda}^{208}\text{Pb}$  is almost ten times larger than that of  ${}_{\Lambda}^{12}\text{C}$  or  ${}_{\Lambda}^{16}\text{O}$ . This is an indication of the energy resolution required to do  $\gamma$  spectroscopy in heavy hypernuclei. A second remark, more related to the aim of our investigation, is that

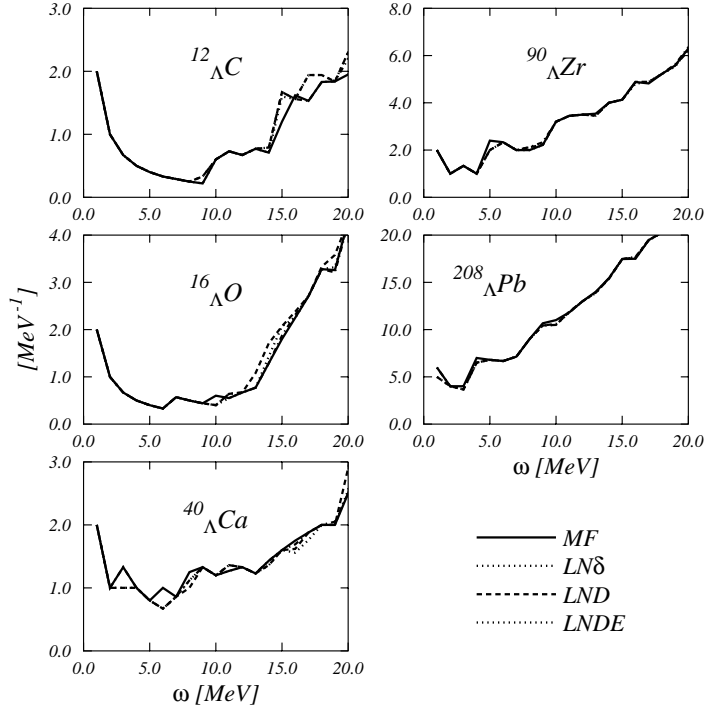


Figure 5: Densities of states as a function of the excitation energy.

the differences between the various lines seem to be more evident for light hypernuclei than for the heavier ones. This could indicate that the MF approach becomes more reliable the heavier is the hypernucleus, or in other words, that collective effects are more inhibited in heavy hypernuclei than in the light ones.

In order to investigate this issue, we have calculated the normalized energy shift with respect to the MF energy,

$$\Delta E = \sum_J \left( \frac{1}{N_J} \sum_i^S \frac{|\omega_i^{J,\text{RPA}} - \omega_i^{J,\text{MF}}|}{|\omega_i^{J,\text{RPA}} + \omega_i^{J,\text{MF}}|} \right), \quad (36)$$

where we have indicated with  $N_J$  the number of multipole excitations we have considered, and the index  $i$  runs on all the  $S$  solutions having the same multipolarity. The above equation is meaningful since, as we have already mentioned, our model produces the same number of excited states in both MF and RPA-like calculations, therefore we can identify the energy shift of each MF solution. We show in Tab. 9 the  $\Delta E$  values obtained for the various  $\Lambda$ -nucleon interactions. These results indicate that the deviations from the MF model are less important, the heavier is the nucleus.

We have compared the values of the hyperonic energy differences of Tab. 9 with analogous values calculated for excitations of ordinary nuclei. The RPA calculations for the doubly magic nuclei have been done with the zero-range Landau-Migdal interaction of Ref. [45]. This comparison indicates that collectivity in hypernuclei is much smaller than in ordinary nuclei. The  $\Delta E$  values for ordinary nuclei are about five times larger than the analogous values obtained for hypernuclei.

	$J_{\max}$	LN $\delta$	LND	LNDE
${}_{\Lambda}^{12}\text{C}$	5	$0.23 \pm 0.07$	$0.26 \pm 0.08$	$0.22 \pm 0.06$
${}_{\Lambda}^{16}\text{O}$	4	$0.33 \pm 0.10$	$0.30 \pm 0.09$	$0.11 \pm 0.03$
${}_{\Lambda}^{40}\text{Ca}$	4	$0.15 \pm 0.04$	$0.12 \pm 0.04$	$0.24 \pm 0.07$
${}_{\Lambda}^{90}\text{Zr}$	6	$0.10 \pm 0.02$	$0.13 \pm 0.03$	$0.09 \pm 0.02$
${}_{\Lambda}^{208}\text{Pb}$	10	$0.10 \pm 0.02$	$0.13 \pm 0.02$	$0.09 \pm 0.01$

Table 9: Renormalized energy differences Eq. (36). We have also indicated the maximum value of the angular momentum of the multipole excitation.

## 5 Summary and conclusions

In this article we have investigated the possible presence of collective phenomena, beyond the MF model description of hypernuclei. To this purpose we have developed a particle-hole model where the formation of the hypernucleus is described as the excitation of a nucleon into a single particle state describing the  $\Lambda$ , and the hypernucleus state is a linear combination of elementary single particle excitations, the coefficients of the combinations being determined by the residual  $\Lambda$ -nucleon interaction. Our model is inspired by the RPA theory and considers some ground state correlations which can be described in terms of  $\Lambda$ -nucleon excitations. Purely nucleonic correlations, such as those considered by the traditional RPA theory, are not included.

Our calculations have been done by using a discrete single particle configuration space, and with three  $\Lambda$ -nucleon interactions with different properties. Since we have been interested in the low energy part of the spectrum, we have checked the stability of our results with respect to the size of the configuration space, and therefore the scarce relevance of a detailed treatment of the continuum.

When possible we have compared our results with those obtained by other calculations. We obtained a reasonable agreement in  ${}_{\Lambda}^{12}\text{C}$  and  ${}_{\Lambda}^{16}\text{O}$ , not only for the energies [41, 42], but also for the electromagnetic B-values with shell model results [43, 39]. For the  ${}_{\Lambda}^{40}\text{Ca}$  hypernucleus, the comparison with the shell model spectrum of Ref. [44] is not so satisfactory. We have the same clustering of states in the spectrum, but we often obtain an inversion of states within the cluster.

Concerning the comparison with the experimental data, we obtain a reasonable agreement with the energies measured in  ${}_{\Lambda}^{16}\text{O}$ . Our model is unable to predict two states observed in  ${}_{\Lambda}^{12}\text{C}$  because it does not consider the partial occupation of the  $1p_{1/2}$  neutron state. The energy resolution of  ${}_{\Lambda}^{40}\text{Ca}$  data [37, 1] does not allow a meaningful comparison with our results. For the  ${}_{\Lambda}^{90}\text{Zr}$  and  ${}_{\Lambda}^{208}\text{Pb}$  hypernuclei we made a comparison with data analyzed in terms of excitation of a single neutron [4, 2]. The agreement with  ${}_{\Lambda}^{90}\text{Zr}$  data is satisfactory, while for the  ${}_{\Lambda}^{208}\text{Pb}$  case there are some problems regarding the spacing between the first two states.

To investigate the presence of collective effects in the spectra of hypernuclei, we have calculated the form factors of the transition producing the hypernucleus and we have compared MF and our RPA-like results. In few cases we have found remarkable differences, however, in all the cases but one, these differences could be explained by considering the excited state as combination of only two single particle transitions. This is not really what we would call a collective behavior of the system. The only situation standing out of this trend is that of the  $0^+$  excitation in  ${}_{\Lambda}^{16}\text{O}$  around 10 MeV, which seems to have a more collective structure.

The energy shifts with respect to the MF results are indicators of effects coming from the  $\Lambda$ -nucleon interaction, and possibly of collective phenomena. Densities of states and average energy shifts do not show remarkable features beyond the MF approach. In our calculations the differences between MF and our RPA-like results become smaller the heavier is the hypernucleus. This is an indication that perturbation effects produced by the  $\Lambda$  on the nuclear systems are better averaged in a heavy system.

The average energy shifts for hypernuclear excitations are, at most, 20% of the shifts obtained for the excitation of a purely nucleonic system. This result is almost independent of the number of nucleons involved, and indicates that in hypernuclear excitation, effects beyond the MF are much less important

than in the excitation of the ordinary nuclear system.

Our model can be further improved in several ways. One of them consists in performing self-consistent calculations, where the single particle basis is generated in a Hartree-Fock approach, with the same  $\Lambda$ -nucleon interaction used in the RPA-like calculations. Other improvements can be obtained by considering nucleonic correlations in the ground state. This could be done in terms of hole-particle excitations, as in the ordinary RPA, in terms of partial occupation probability of the nucleonic single particle states, as it happens in the quasi-particle RPA, and also by considering explicitly the short-range correlations as in Ref. [36].

## ACKNOWLEDGMENTS

We thank B. Dalena for useful discussions.

## Appendix

In this appendix we give the expressions of the matrix elements (16) and (17) of the secular RPA-like equations for all the terms of the interaction (19).

For the scalar term  $V_{\Lambda N}^c$  we obtain the expressions

$$\begin{aligned}
v_{c,\Lambda h\Lambda' h'}^{J,dir} &= \frac{2}{\pi} \int dq q^2 F_{\Lambda}(q) \int dr_1 r_1^2 R_{\Lambda}^*(r_1) R_h(r_1) j_J(qr_1) \\
&\quad \int dr_2 r_2^2 R_{h'}^*(r_2) R_{\Lambda'}(r_2) j_J(qr_2) \\
&\quad \frac{(-1)^{j_{\Lambda}+j_{\Lambda'}+1}}{4\pi} \hat{j}_{\Lambda} \hat{j}_h \hat{j}_{\Lambda'} \hat{j}_{h'} \begin{pmatrix} j_{\Lambda} & J & j_h \\ \frac{1}{2} & 0 & -\frac{1}{2} \end{pmatrix} \begin{pmatrix} j_{h'} & J & j_{\Lambda'} \\ \frac{1}{2} & 0 & -\frac{1}{2} \end{pmatrix} \\
&\quad \xi(l_{\Lambda} + l_h + J) \xi(l_{\Lambda'} + l_{h'} + J) ,
\end{aligned} \tag{37}$$

and

$$\begin{aligned}
v_{c,\Lambda h\Lambda' h'}^{J,exch} &= \frac{2}{\pi} \sum_l \int dq q^2 F_{\Lambda}(q) \int dr_1 r_1^2 R_{\Lambda}^*(r_1) R_{\Lambda'}(r_1) j_l(qr_1) \\
&\quad \int dr_2 r_2^2 R_{h'}^*(r_2) R_h(r_2) j_l(qr_2) \\
&\quad \frac{(-1)^{j_{\Lambda}+j_{\Lambda'}+J+l}}{4\pi} \hat{j}_{\Lambda} \hat{j}_h \hat{j}_{\Lambda'} \hat{j}_{h'} \hat{l}^2 \begin{pmatrix} j_{\Lambda} & l & j_{\Lambda'} \\ \frac{1}{2} & 0 & -\frac{1}{2} \end{pmatrix} \begin{pmatrix} j_{h'} & l & j_h \\ \frac{1}{2} & 0 & -\frac{1}{2} \end{pmatrix} \\
&\quad \left\{ \begin{matrix} j_{\Lambda} & j_h & J \\ j_{h'} & j_{\Lambda'} & l \end{matrix} \right\} \xi(l_{\Lambda} + l_{\Lambda'} + l) \xi(l_h + l_{h'} + l) .
\end{aligned} \tag{38}$$

In the above equations we have indicated with  $R(r)$  the radial part of the single particle wave functions, with  $j_l(qr)$  the spherical Bessel functions, and with the traditional symbols the Wigner three and six  $j$  coefficients [18].

The analogous expressions for the spin-dependent terms are

$$\begin{aligned}
v_{\sigma, \Lambda h \Lambda' h'}^{J, dir} &= \frac{2}{\pi} \sum_l \int dq q^2 G_\Lambda(q) \int dr_1 r_1^2 R_\Lambda^*(r_1) R_h(r_1) j_l(qr_1) \\
&\quad \int dr_2 r_2^2 R_{h'}^*(r_2) R_{\Lambda'}(r_2) j_l(qr_2) \\
&\quad (-1)^{l+J+l_\Lambda+l_{h'}+j_{\Lambda'}+j_h} \frac{3}{2\pi} \hat{l}^2 \hat{l}_\Lambda \hat{l}_h \hat{l}_{\Lambda'} \hat{l}_{h'} \hat{j}_\Lambda \hat{j}_h \hat{j}_{\Lambda'} \hat{j}_{h'} \\
&\quad \left\{ \begin{matrix} l_\Lambda & \frac{1}{2} & j_\Lambda \\ l_h & \frac{1}{2} & j_h \\ l & 1 & J \end{matrix} \right\} \left\{ \begin{matrix} l'_\Lambda & \frac{1}{2} & j'_\Lambda \\ l'_h & \frac{1}{2} & j'_h \\ l & 1 & J \end{matrix} \right\} \begin{pmatrix} l_\Lambda & l & l_h \\ 0 & 0 & 0 \end{pmatrix} \begin{pmatrix} l'_\Lambda & l & l_{h'} \\ 0 & 0 & 0 \end{pmatrix}, \quad (39)
\end{aligned}$$

and

$$\begin{aligned}
v_{\sigma, \Lambda h \Lambda' h'}^{J, exch} &= \frac{2}{\pi} \sum_l \int dq q^2 G_\Lambda(q) \int dr_1 r_1^2 R_\Lambda^*(r_1) R_{\Lambda'}(r_1) j_l(qr_1) \\
&\quad \int dr_2 r_2^2 R_{h'}^*(r_2) R_h(r_2) j_l(qr_2) \\
&\quad \sum_L \frac{3}{2\pi} (-1)^{l_\Lambda+l_{h'}+j_{\Lambda'}+j_h+l+J+1} \\
&\quad \hat{l}_\Lambda \hat{l}_h \hat{l}_{\Lambda'} \hat{l}_{h'} \hat{j}_\Lambda \hat{j}_h \hat{j}_{\Lambda'} \hat{j}_{h'} \hat{l}^2 \hat{L}^2 \left\{ \begin{matrix} j_\Lambda & j_h & J \\ j_{h'} & j_{\Lambda'} & L \end{matrix} \right\} \\
&\quad \left\{ \begin{matrix} l_\Lambda & \frac{1}{2} & j_\Lambda \\ l_h & \frac{1}{2} & j_h \\ l & 1 & L \end{matrix} \right\} \left\{ \begin{matrix} l'_\Lambda & \frac{1}{2} & j'_\Lambda \\ l'_h & \frac{1}{2} & j'_h \\ l & 1 & L \end{matrix} \right\} \begin{pmatrix} l_\Lambda & l & l_{\Lambda'} \\ 0 & 0 & 0 \end{pmatrix} \begin{pmatrix} l_h & l & l_{h'} \\ 0 & 0 & 0 \end{pmatrix}. \quad (40)
\end{aligned}$$

For the tensor components of the interaction we obtain:

$$\begin{aligned}
v_{t, \Lambda h \Lambda' h'}^{J, dir} &= \frac{2}{\pi} \sum_{l_1 l_2} \int dq q^2 H_\Lambda(q) \int dr_1 r_1^2 R_\Lambda^*(r_1) R_h(r_1) j_{l_1}(qr_1) \\
&\quad \int dr_2 r_2^2 R_{h'}^*(r_2) R_{\Lambda'}(r_2) j_{l_2}(qr_2) \\
&\quad \frac{3\sqrt{30}}{2\pi} (-1)^{j_{\Lambda'}+j_{h'}+l_\Lambda+l_{h'}} \hat{l}_\Lambda \hat{l}_h \hat{l}_{\Lambda'} \hat{l}_{h'} \hat{j}_\Lambda \hat{j}_h \hat{j}_{\Lambda'} \hat{j}_{h'} \\
&\quad (-1)^{\frac{3}{2}(l_1+l_2)} \hat{l}_1^2 \hat{l}_2^2 \begin{pmatrix} l_1 & l_2 & 2 \\ 0 & 0 & 0 \end{pmatrix} \begin{pmatrix} l_\Lambda & l_1 & l_h \\ 0 & 0 & 0 \end{pmatrix} \begin{pmatrix} l_{h'} & l_2 & l_{\Lambda'} \\ 0 & 0 & 0 \end{pmatrix} \\
&\quad \left\{ \begin{matrix} l_1 & l_2 & 2 \\ 1 & 1 & J \end{matrix} \right\} \left\{ \begin{matrix} l_\Lambda & \frac{1}{2} & j_\Lambda \\ l_h & \frac{1}{2} & j_h \\ l_1 & 1 & J \end{matrix} \right\} \left\{ \begin{matrix} l_{h'} & \frac{1}{2} & j_{h'} \\ l_{\Lambda'} & \frac{1}{2} & j_{\Lambda'} \\ l_2 & 1 & J \end{matrix} \right\}, \quad (41)
\end{aligned}$$

for the direct term, and for the exchange term we get the expression

$$\begin{aligned}
v_{t, \Lambda h \Lambda' h'}^{J, exch} &= -\frac{2}{\pi} \sum_{l_1 l_2} \int dq q^2 H_\Lambda(q) \int dr_1 r_1^2 R_\Lambda^*(r_1) R_{\Lambda'}(r_1) j_{l_1}(qr_1) \\
&\quad \int dr_2 r_2^2 R_{h'}^*(r_2) R_h(r_2) j_{l_2}(qr_2) \\
&\quad \frac{3\sqrt{30}}{\pi^2} (-1)^{l_\Lambda+l_{h'}+j_{\Lambda'}+j_h+l_1+l_2+J} \hat{l}_1^2 \hat{l}_2^2 \\
&\quad \hat{l}_\Lambda \hat{l}_h \hat{l}_{\Lambda'} \hat{l}_{h'} \hat{j}_\Lambda \hat{j}_h \hat{j}_{\Lambda'} \hat{j}_{h'} \hat{l}_1^2 \hat{l}_2^2
\end{aligned}$$

$$\begin{aligned}
& \begin{pmatrix} l_1 & l_2 & 2 \\ 0 & 0 & 0 \end{pmatrix} \begin{pmatrix} l_\Lambda & l_1 & l_{\Lambda'} \\ 0 & 0 & 0 \end{pmatrix} \begin{pmatrix} l_{h'} & l_2 & l_\Lambda \\ 0 & 0 & 0 \end{pmatrix} \\
& \sum_L (-1)^L \hat{L}^2 \begin{Bmatrix} l_1 & l_2 & 2 \\ 1 & 1 & L \end{Bmatrix} \begin{Bmatrix} j_\Lambda & j_h & J \\ j_{h'} & j_{\Lambda'} & L \end{Bmatrix} \\
& \begin{Bmatrix} l_\Lambda & \frac{1}{2} & j_\Lambda \\ l_h & \frac{1}{2} & j_h \\ l_1 & 1 & L \end{Bmatrix} \begin{Bmatrix} l_{h'} & \frac{1}{2} & j_{h'} \\ l_{\Lambda'} & \frac{1}{2} & j_{\Lambda'} \\ l_2 & 1 & L \end{Bmatrix}. \tag{42}
\end{aligned}$$

## References

- [1] P. H. Pile, et al., Phys. Rev. Lett. 66 (1991) 2585.
- [2] T. Hasegawa, et al., Phys. Rev. C 53 (1996) 1210.
- [3] S. Ajimura, et al., Nucl. Phys. A 639 (1998) 93.
- [4] H. Hotchi, et al., Phys. Rev. C 64 (2001) 044302.
- [5] H. Tamura, R. S. Hayano, H. Outa, Y. Yamazaki, Prog. Theor. Phys. Suppl. 117 (1994) 1.
- [6] M. Agnello, et al., Phys. Lett. B 622 (2005) 35.
- [7] M. Agnello, et al., Nucl. Phys. A 754 (2005) 399c.
- [8] T. Miyoshi, et al., Phys. Rev. Lett. 90 (2003) 232502.
- [9] F. Garibaldi, Eur. Phys. J. A 24S1 (2005) 91.
- [10] M. Iodice, et al., Phys. Rev. Lett. 99 (2007) 052501.
- [11] O. Hashimoto, H. Tamura, Prog. Part. Nucl. Phys. 57 (2006) 564.
- [12] Y. Ma, et al., Eur. Phys. J. A 33 (2007) 243.
- [13] N. Auerbach, N. V. Giai, S. Y. Lee, Phys. Lett. B 68 (1977) 225.
- [14] M. T. López-Arias, Nucl. Phys. A 582 (1995) 440.
- [15] D. J. Rowe, Nuclear Collective Motion: models and theory, Meuthen, London, 1970.
- [16] A. L. Fetter, J. D. Walecka, Quantum theory of many-particle systems, McGraw-Hill, S. Francisco, 1971.
- [17] P. Ring, P. Schuck, The nuclear many-body problem, Springer, Berlin, 1980.
- [18] A. R. Edmonds, Angular momentum in quantum mechanics, Princeton University Press, Princeton, 1957.
- [19] J. Suhonen, From nucleons to nucleus, Springer, Berlin, 2007.
- [20] J. M. Blatt, V. F. Weisskopf, Theoretical nuclear physics, John Wiley and sons, New York, 1952.
- [21] A. Bohr, B. R. Mottelson, Nuclear structure, vol. I, Benjamin, New York, 1969.
- [22] A. Migdal, Theory of finite Fermi systems and applications to atomic nuclei, Interscience, London, 1967.

- [23] J. Speth, E. Werner, W. Wild, *Phys. Rep.* 33 (1977) 127.
- [24] F. Grümmer, J. Speth, *Jour. Phys. G* 32 (2006) R193.
- [25] F. Arias de Saavedra, C. Bisconti, G. Co', A. Fabrocini, *Phys. Rep.* 450 (2007) 1.
- [26] D. J. Millener, C. B. Dover, A. Gal, *Phys. Rev. C* 38 (1988) 2700.
- [27] D. J. Millener, *Nucl. Phys. A* 754 (2005) 48c.
- [28] T. Sil, S. Shlomo, B. K. Agrawal, P. G. Reinhard, *Phys. Rev. C* 73 (2006) 034316.
- [29] Y. Yamamoto, H. Bandō, *Prog. Theor. Phys.* 73 (1985) 905.
- [30] H. Bandō, T. Motoba, J. Žofka, *Int. J. Mod. Phys. A* 5 (1990) 4021.
- [31] O. Hashimoto, et al., *Nucl. Phys. A* 639 (1998) 93c.
- [32] M. Ukai, et al., *Phys. Rev. Lett.* 93 (2004) 232501.
- [33] M. Ukai, et al., *Eur. Phys. J. A* 33 (2007) 247.
- [34] M. M. Nagels, T. A. Rijken, J. J. de Swart, *Phys. Rev. D* 20 (1979) 1633.
- [35] K. Nakayama, S. Krewald, J. Speth, *Phys. Lett. B* 148 (1984) 399.
- [36] F. Arias de Saavedra, G. Co', A. Fabrocini, *Phys. Rev. C* 63 (2001) 064308.
- [37] W. Bruckner, et al., *Phys. Lett. B* 79 (1978) 157.
- [38] R. H. Dalitz, *Nucl. Phys. A* 450 (1986) 311c.
- [39] D. J. Millener, *Topics in Strangeness Nuclear Physics*, P. Bydžovský, A. Gal and J. Mareš (Eds.), Springer, Berlin, 2007.
- [40] H. Tamura, et al., *Nucl. Phys. A* 754 (2005) 58c.
- [41] K. Itonaga, T. Motoba, O. Richter, M. Sotona, *Phys. Rev. C* 49 (1994) 1045.
- [42] D. J. Millener, *Nucl. Phys. A* 691 (2001) 93.
- [43] R. H. Dalitz, A. Gal, *Ann. Phys. (NY)* 116 (1978) 167.
- [44] Y. Tzeng, S. Y. T. Tzeng, T. T. S. Kuo, *Phys. Rev. C* 65 (2002) 047303.
- [45] G. A. Rinker, J. Speth, *Nucl. Phys. A* 306 (1978) 360.